Short communication: Multiscalar drag decomposition in fluvial systems using a transform-roughness correlation (TRC) approach

David L. Adams[1,2] and Andrea Zampiron[3]

[1]Department of Geography, The University of British Columbia, Vancouver, BC, Canada
[2]School of Geography, The University of Melbourne, Melbourne, VIC, Australia
[3]Department of Mechanical Engineering, The University of Melbourne, Melbourne, VIC, Australia

Correspondence: David L. Adams (dladams@alumni.ubc.ca)

Abstract.

In natural open-channel flows over complex surfaces, a wide range of superimposed roughness elements may contribute to flow resistance. Gravel-bed rivers present a particularly interesting example of this kind of multiscalar flow resistance problem, as both individual grains and bedforms can potentially be important roughness elements. In this paper, we propose a novel
5 method of estimating the relative contribution of different physical scales of river bed topography to the total drag, using a transform-roughness correlation (TRC) approach. The technique, which requires only a single longitudinal profile, consists of (1) a wavelet transform which decomposes the surface into roughness elements occurring at different wavelengths, and (2) a 'roughness correlation' that estimates the drag associated with each wavelength based on its geometry alone, expressed as k_s. We apply the TRC approach to original and published laboratory experiments and show that the multiscalar drag decomposition
10 yields estimates of grain- and form-drag that are consistent with estimates in channels with similar morphologies. Also, we demonstrate that the roughness correlation may be used to estimate total flow resistance via a conventional equation, suggesting that it could replace representative roughness values such as median grain size or the standard deviation of elevations. An improved understanding of how various scales contribute to total flow resistance may lead to advances in hydraulics as well as channel morphodynamics.

15 ## 1 Introduction

Understanding flow resistance is of great interest to river research and practice. The estimation of flow resistance is important for determining flood magnitudes, predicting ecological habitat, and understanding the morphodynamic behaviour of channels. However, the hydraulics of gravel-bed channels, in particular, are relatively poorly understood due to a range of factors (see Ferguson, 2007). Given that most of the foundational work in fluid dynamics, upon which conventional approaches to predict-
20 ing flow resistance are based, was conducted using regular (e.g., Schlichting, 1936) or uniscalar (e.g., Nikuradse, 1933) bed geometry, the multiscalar topographic characteristics of these rivers presents a major challenge. In particular, both individual grains and bedforms on the bed surface, spanning orders-of-magnitude of scale, may contribute to the total flow resistance (see Adams, 2020a). Researchers have been aware of these limitations for over half-a-century (Sundborg, 1956; Leopold et al., 1964), and have used empirically derived coefficients to account for the multiple scales of roughness present (Chow, 1959; Hey,

25   1979), although such an approach has considerable limitations (Ferguson, 2007; Adams, 2020a). There have also been more mechanistic attempts to disaggregate flow resistance, primarily into 'grain' (small-scale) and 'form' (large-scale) components (Parker and Peterson, 1980; Prestegaard, 1983; Hey, 1988; Weichert et al., 2009).

Advances in remote-sensing and statistics have allowed researchers to explore detailed scaling characteristics of gravel-bed surfaces using structure-functions (Furbish, 1987; Robert and Richards, 1988; Robert, 1991; Clifford et al., 1992), filtering
30   (Bergeron, 1996), and transforms (Nyander et al., 2003). This approach to analyzing river beds has led to multiscalar decompositions of geometric roughness, rather than direct decompositions of hydraulic roughness. The latter approach has been developed for complex aeolian surfaces using transforms (Nield et al., 2013; Pelletier and Field, 2016; Field and Pelletier, 2018), which serves as a proof-of-concept for the multiscalar drag decomposition approach.

Also, as high-resolution spatial information becomes increasingly available to geomorphologists working in both laboratory
35   and field environments (Westoby et al., 2012), there is a general need for statistical representations that effectively summarise these large datasets in a way that is informed by theory. Moreover, as energy-balance is increasingly recognized as a condition governing channel behaviour (Eaton and Church, 2004, 2009; Nanson and Huang, 2008, 2018; Church, 2015), improved understanding of flow resistance may contribute to a broader understanding of fluvial systems.

In a review of flow resistance in gravel-bed rivers, Adams (2020a) identified two relatively recent advancements in the fields
40   of statistics and fluid dynamics that could contribute to a multiscalar drag decomposition tool. The first advancement is the wavelet transform, which is generally superior to the Fourier transform when analysing the underlying structure of complex and aperiodic signals, due to its use of a finite analysing function ('the wavelet') rather than a continuous one (Torrence and Compo, 1998). There are now various types of wavelet transform suited to different applications, some of which have been applied in rivers (Kumar and Foufoula-Georgiou, 1997; Nyander, 2004; Keylock et al., 2014). The second advancement is
45   the development of roughness correlations for irregular surfaces (e.g. Forooghi et al., 2017), which estimate the fluid drag generated by a surface based purely on its geometric characteristics.

In this piece, we present a novel method of estimating the relative contribution of different physical scales of river bed topography to the total drag, using only a single longitudinal profile. The general approach consists of (1) a wavelet transform in which the channel surface is decomposed into a set of more simple components each at a different wavelength, and (2)
50   a roughness correlation that estimates the drag associated with each wavelength, which is expressed as the equivalent sand roughness parameter k_s (Nikuradse, 1933; Schlichting, 1936). By modifying the specific roughness correlation that is used, the transform-roughness correlation (TRC) approach may be applied in a wide range of hydraulic conditions. To demonstrate this tool, we present code in R language and apply it to a series of original laboratory experiments with high-resolution digital elevation models (DEMs), as well as some additional published data. Multiscalar drag decomposition provides researchers
55   with useful information as they approach challenges pertaining to flow resistance and channel morphodynamics.

2 Methodological considerations

The transform-roughness correlation approach is a generic tool that should be adapted based on the hydraulic conditions and the purpose of its application. These considerations should span the data that is used, the type of wavelet transform, and the specific roughness correlation that is selected. We discuss these general considerations first as they provide context for the TRC approach.

First, the minimum resolution and spatial extent of the topographic dataset should be informed by the scale of the features of interest. The data should have a sufficiently small spatial resolution such that it can capture the range of bed features that contribute to drag. Also, to capture the characteristic geometry of bed features, the spatial extent of the dataset should be at least the length of the largest features that produce significant drag, for example, it should span many dunes crests or pool-riffle pairs.

Second, given that hydraulic roughness is of interest, the data could be reduced to streamlines representing primary flow paths. In some contexts, it may be acceptable to simplify the in-channel area to a one-dimensional profile extending along the thalweg, given that this should represent the surface that most of the flow interacts with. Alternatively, if the range of interactions between the flow and the surface is of interest, multiple streamlines (parallel or even intersecting) could be employed.

Third, the choice of wavelet transform in this context is a trade-off between the resolution of the decomposition and the ability to interpret it. The maximal overlap discrete wavelet transform (MODWT) offers several advantages over the discrete wavelet transform (DWT) and facilitates alignment between the original signal and the decomposition. The continuous wavelet transform (CWT) extracts more intricate structural characteristics from the original data and yields a greater number of wavelengths between which information is shared (Addison, 2018). However, the CWT generates a more abstract representation of the topographic variation at a given wavelength. A comparison of wavelengths extracted using MODWT and CWT methods is presented in Figure 1. At the wavelength corresponding to the spacing of a pool-bar-riffle sequence ($\lambda \approx 2$ m), the MODWT is aligned with the original thalweg elevation profile, but the CWT is not. Given that the CWT wavelengths do not resemble the original data, interpreting the results of roughness correlation applied to these wavelengths may be more difficult, and such results may be entirely invalid.

Fourth, the specific roughness correlation should match the channel's boundary Reynolds number $Re^* = U^*k/v$, where U^* is shear velocity, k is some representative roughness scale, and v is kinematic viscosity. Given that the fluid dynamics characteristic of different boundary Reynolds numbers are highly varied, roughness correlations have only been developed for relatively limited ranges of Re^*. For example, given that gravel-bed rivers tend to be within the fully rough regime where $Re^* \geq 70$ (Buffington and Montgomery, 1997; Schlichting, 1979), it may only be valid to apply roughness correlations obtained for that regime specifically. Also, the flow should be turbulent, and it should be two-dimensional, indicated by flow aspect ratios (w/h, where w is the wetted width and h is flow depth) greater than 5 (Nezu and Nakagawa, 1993).

Last, roughness correlations in fluid dynamics tend to be developed for flows sufficiently deep to have logarithmic velocity profiles, which should be considered when they are applied to flows with less developed profiles. Jimenez (2004) suggested that logarithmic layers develop where relative submergence h/k is greater than 40, although Cameron et al. (2017) observed
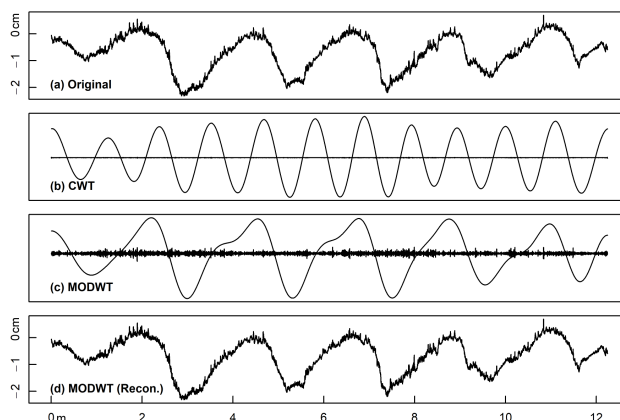
3

Figure 1. a) Thalweg elevation profile at end of Experiment 1a featuring a prominent pool-riffle sequence, where the x-axis represents distance upstream, b) grain ($\lambda = 4$ mm) and form ($\lambda \approx 2$ m) wavelengths derived from CWT, c) the same two wavelengths derived from a MODWT, and d) the original signal reconstructed from the MODWT by recombining wavelengths.

90 a logarithmic layer in rough open-channel flow at submergences as low as 1.9. During most flow conditions, it is common for gravel-bed rivers to have relative submergences of less than 10, and in some cases, as low as 0.1 (Lee and Ferguson, 2002; Ferguson, 2007), where no logarithmic layer can develop because roughness elements are not submerged. However, if one is interested in channel-forming flows capable of reworking the bed surface (Ashworth and Ferguson, 1989; Wolman and Miller, 1960) where relative submergence may be two orders of magnitude higher (Limerinos, 1970; Griffiths, 1981; Bray, 1982; 95 Millar, 1999), the logarithmic assumption should be satisfied for most rivers.

3 Application of TRC approach in gravel-bed rivers

3.1 Stream table experiment

To demonstrate the TRC approach, we required a large set of DEMs and associated hydraulic data for validation. We conducted a set of experiments using the Adjustable-Boundary Experimental System (A-BES) at the University of British Columbia 100 (Figure 2). The A-BES comprises a 1.75 m wide by 12.2 m long tilting stream table, and a recirculating water pump. The experiments were run as generic Froude-scaled models with an initial bed slope of 2 percent and a length scale ratio of 1:25, based on field measurements from steep gravel-bed rivers in Alberta, Canada. The bulk material ranged from 0.25 to 8 mm (D_{max}), with a D_{50} of 1.6 mm and D_{90} of 3.9 mm (see MacKenzie and Eaton, 2017). The banks were lined with roughly-cast interlocking concrete bricks to make a straight channel. Ten stream gages were equally spaced along the inner edge of the 105 bricks.

Earth **Surface**
Dynamics
Discussions

EGU

Figure 2. Adjustable-Boundary Experimental System (A-BES) at the University of British Columbia, showing the camera rig and the 30 cm wide channel configuration.

Table 1. Summary of experimental conditions in the A-BES.

Run	Width W (m) ($\pm$ 0.02)	Discharge Q (L/s) ($\pm$ 0.03)	Duration (hrs)	DEMs
Exp1a	0.3	1.5	16	24
Exp1b	0.3	1.0	16	24
Exp1c	0.3	0.67, 1.0, 1.5, 2.25	8, 4, 4, 4	68
Exp2a	0.08	0.4	16	24
Exp2b	0.08	0.27	16	24

3.1.1 Experimental procedure

The bricks were configured to make two different widths: (1) a 30 cm wide configuration that represents the scaled bankfull width of the field prototype, and (2) an 8 cm wide configuration which was selected based on preliminary experiments where channel width was decreased until bar formation was suppressed entirely. Thus, the two widths yield a range of bed morpholo-
110 gies and hydraulic conditions. A set of experiments were carried out for each configuration (Table 1). The first experiment ('a') consisted of a bankfull equivalent flow for the prototype for 16 hours, where the discharge was scaled with the width of the experimental channel W. The second experiment ('b') consisted of a flow two-thirds of the bankfull equivalent for 16 hours. The third experiment ('c'), conducted for the 30 cm wide channel only, consisted of low flow for 8 hours, and then three 4 hour phases with discharge increasing by a factor of 1.5 each time.
115   Before each experiment, the bulk material was hand-mixed to minimize downstream and lateral sorting, and the channel area was screeded to the height of the weirs at the upstream and downstream end. The flow was run at a low rate until the bed was fully saturated, and was then increased to the target flow. Each period of constant discharge was divided into phases of increasing duration, between which the bed was drained and photographed. Phases for the 16-hour experiments consisted of 5,

Table 2. Summary of A-BES experimental data collected during the final portion of each experimental phase. Values represent the mean of the last five measurements. Re^* was calculated with $k = k_{s,pred}^*$.

Exp	W	Q	h	F_r	U	U^*	U/U^*	σ_z	h/σ_z	Re^*	$k_{s,pred}^*$	$h/k_{s,pred}^*$
Exp1a	0.30	1.50	0.014	0.95	0.36	0.053	6.76	0.0057	2.53	136	0.0034	4.32
Exp1b	0.30	1.00	0.012	0.85	0.29	0.049	6.00	0.0056	2.17	120	0.0032	3.72
Exp1c(1)	0.30	0.67	0.012	0.59	0.20	0.048	4.17	0.0051	2.27	105	0.0029	4.10
Exp1c(2)	0.30	1.00	0.013	0.70	0.25	0.051	4.96	0.0067	2.02	152	0.0039	3.47
Exp1c(3)	0.30	1.50	0.014	0.90	0.33	0.052	6.40	0.0063	2.24	154	0.0039	3.65
Exp1c(4)	0.30	2.25	0.018	1.03	0.43	0.060	7.28	0.0033	5.49	86	0.0019	9.79
Exp2a	0.08	0.40	0.015	0.92	0.35	0.054	6.47	0.0025	6.94	73	0.0018	11.55
Exp2b	0.08	0.27	0.013	0.75	0.26	0.050	5.29	0.0019	6.96	76	0.0020	7.34

10, 15, 30, 60, and 120 minutes, with four repeats of each. The 4 and 8 hour periods of constant discharge followed the same
120 sequence but did not include the longest phases. In the final 30 seconds of each phase, the water surface elevation was recorded at each gage to the nearest 1 mm. Given that most of the maximum flow depths that were measured were greater than 15-20 mm, this degree of precision yields errors of approximately ± 10 percent.

The camera rig consisted of five Canon EOS Rebel T6i DSLRs with EF-S 18-55 mm lenses positioned at oblique angles in the cross-stream direction to maximise coverage of the bed, and five LED lights. Photos were taken in RAW format at 20 cm
125 intervals, yielding a stereographic overlap of over two-thirds. Throughout the experiment, sediment collected in the trap was drained of excess water, weighed wet to the nearest 0.2 kg, placed on the conveyor belt at the upstream end, and recirculated at the same rate it was output. Zero sediment was fed into the system during the first 5-minute phase. For the five- and ten-minute phases, recirculation occurred at the end of the phase, and for the phases of longer duration, recirculation occurred every 15 minutes regardless of whether the bed was drained.

130 **3.1.2 Data processing**

Using the images, LAS point clouds were produced with Agisoft MetaShape Professional 1.6.2 at the highest resolution, yielding an average point spacing of less than 0.5 mm. Twelve spatially-referenced control points (and additional unreferenced ones) were distributed throughout the A-BES, which placed photogrammetric reconstructions within a local coordinates system and aided in the photo-alignment process. The point clouds were imported into RStudio where inverse distance weighting was
135 used to produce DEMs at 1 mm horizontal resolution. Despite the use of control points, the DEM contained a slight arch effect whereby the middle of the model was bowed upwards. This effect was first quantified by applying a quadratic function along the length of the bricks, which represent a linear reference elevation. The arch was then removed by determining correction values along the length of the DEM using the residuals, which were then applied across the width of the model.

The channel thalweg for each DEM was determined by first locating pool centroids using the lowest ten percent of elevations
140 at each cross-section, and then using Gaussian kernel regression to smooth vertices between the centroids. An example of
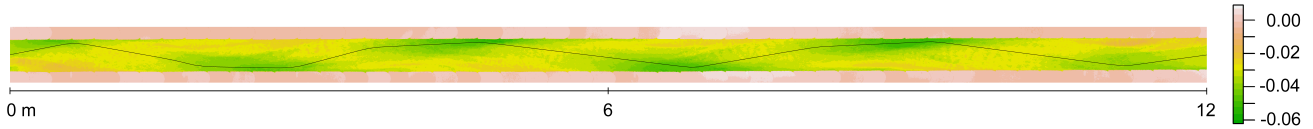
Figure 3. DEM of the channel morphology at the end of Experiment 1a, with estimated position of the thalweg. Zero represents the downstream extent of the model.

the estimated thalweg location is shown in Figure 3. For each DEM, ten wetted cross-sections were reconstructed using the water surface elevation data, which were used to estimate reach-averaged hydraulics. Mean hydraulic depth was calculated as $h = A/w$, where A is cross-sectional area and w is the wetted width. Velocity was estimated using the continuity equation $U = Q/A$. Shear velocity is $U^* = ghS^{1/2}$, where g is gravity and S is slope, and Froude number $Fr = U/(gh)^{1/2}$. A summary
145   of this data is presented in Table 2.

3.1.3   Additional experiments

In addition to the experiments conducted for this study, we obtained topographic and hydraulic data for 86 step-pool experiments published by Hohermuth and Weitbrecht (2018). The experiments were conducted in a 1:20 Froude-scaled model of a mountain stream, utilizing a range of bed slopes (8 – 11 percent), channel widths (15 – 35 cm), and discharges. For a given
150   experiment, a range of potentially usable elevation profiles were identified based on criteria for erroneous values, then the profile closest to the channel centreline was selected. Of the 86 experiments conducted, 83 experiments are used in this study. Thus, there is a total of 247 DEMs with associated hydraulic data when combined with the A-BES experiments.

3.2   The transform-roughness correlation approach

Here we specifically tailor the TRC approach to the geometric and hydraulic characteristics of gravel-bed channels. First, a
155   MODWT is applied to the thalweg elevation profiles of each DEM, yielding a set of simplified profiles representing topographic variation occurring at different wavelengths. Second, a roughness correlation for irregular surfaces in the fully rough regime is applied to each wavelength to estimate the associated drag. Using direct numerical simulation (DNS) in closed channels with systematically generated surface geometries, Forooghi et al. (2017) proposed the following empirical relation

$$\frac{k_s}{k} = F(Sk, \Delta) \cdot F(ES) \tag{1}$$

160   where k is a measure of roughness peak heights, and Sk is the skewness of the probability distribution of elevations. The functions $F(Sk, \Delta)$, $F(Sk)$, and $F(ES)$ are defined, respectively, as

$$F(Sk, \Delta) = \begin{cases} F(Sk), & \Delta \geq 0.35 \\ F(Sk)(1 + m(Sk) \cdot (\Delta - \Delta_0)), & \Delta \leq 0.35 \end{cases} \tag{2}$$

$$F(Sk) = 0.67Sk^2 + 0.93Sk + 1.3 \tag{3}$$

and

$$F(ES) = 1.05 \cdot (1 - e^{-3.8 \cdot ES}) \tag{4}$$

where Δ is a measure of the diversity of roughness peak heights ($\Delta = 0$ if peak heights are identical), $\Delta_0 = 0.35$, and $m(Sk) = 1.47Sk^2 - 1.35Sk - 0.66$. The parameter ES is the effective slope which may be interpreted as the mean gradient of the local roughness elements (Napoli et al., 2008), and is given by

$$ES = \frac{1}{L} \int_L \left| \frac{dz(x)}{dx} \right| dx \tag{5}$$

where $z(x)$ is the height array, x is the streamwise direction, and L is the surface length in x. Effective slope is approximately proportional to drag in the range $0 < ES < 0.35$ (Napoli et al., 2008; Schultz and Flack, 2009). In the TRC approach, calculating the Δ parameter is impractical given that longer topographic wavelengths may contain very few (or even one) complete oscillations that could be interpreted as roughness peaks. As a result, we simply use the $F(Sk)$ term in Equation 2, which is likely appropriate given that for most natural surfaces $\Delta \gg 0$ (Forooghi et al., 2017). In the original equation, k was defined as the peak-to-trough height of the surfaces, however, we adopt the standard deviation of elevations σ_z for the natural surfaces analysed herein as they are more topographically variable than the numerically-generated surfaces, and there is less bias towards extreme peaks and troughs. The effects of different choices of k are briefly explored in Figure 7. The estimated drag for each wavelength is expressed as k_s. The experimental data and code that performs the MODWT and applies the roughness correlation is available online. In the following section, we present the results of the TRC approach applied to the experiments.

4   Results and Discussion

In this section, we primarily focus on the results from Experiment 1a, which features a well-developed pool-riffle-bar sequence formed at a bankfull flow. First, we show how the key parameters of the roughness correlation (effective slope and standard deviation) vary across each wavelength. Second, we estimate the relative contribution of different scales of bed topography to the total drag and explain how the estimated values relate to the key parameters and the characteristics of the experimental surfaces. Third, we perform a sensitivity analysis for the choice of analysing function (known as the 'mother wavelet') in the MODWT and the choice of k in the roughness correlation. Finally, using all of the available experiments, we demonstrate that the roughness correlation may be used to estimate total flow resistance using a conventional equation.
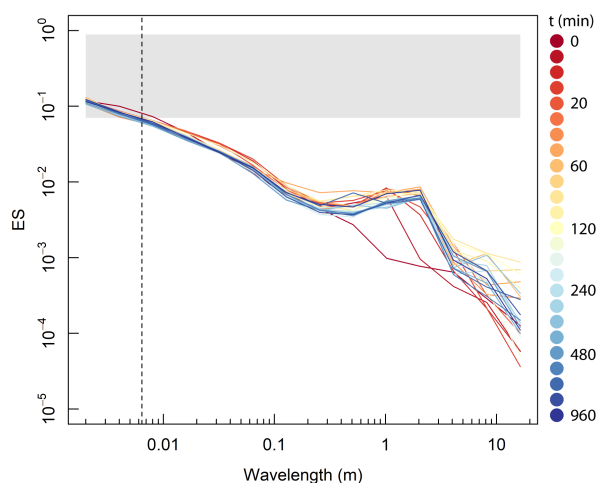
Figure 4. Effective slope of each topographic wavelength during Experiment 1a, where each line represents a point in time. Vertical dashed line represents the largest grain diameter in the experiment. The shaded area represents the range of ES values of the surfaces generated by Forooghi et al. (2017).

Figure 4 shows the effective slope of each topographic wavelength (or spatial scale) over the course of Experiment 1a. The effective slope is greatest at the grain scale wavelengths ($\lambda \leq D_{max}$) where the surface is locally rough and reduces as the wavelength increases and the topography is more locally subdued. This is demonstrated in Figure 1b, where wavelengths at the grain scale have more acute oscillations than those at longer wavelengths. The main exception to this trend is the wavelength of around 2 m where there is a prominent peak in the ES distribution, associated with the development of the pool-riffle-bar sequence approximately ten minutes into the experiment. It is important to note that most of the topographic wavelengths have values of ES (and k_s/k in Equation 1) that are smaller than the surfaces used by Forooghi et al. (2017) to develop the roughness correlation. Thus, it may be more appropriate to focus on the relative values of $k_{s,pred}$ for a specific combination of channel geometry and roughness correlation.

Figure 5a shows the standard deviation of each topographic wavelength for Experiment 1a. Except for the first ten minutes (i.e. first two DEMs) during which the bed morphology is developing, there is a minor peak in σ_z at the scale of 3 cm, and a major peak at the scale of 2 m. At the smallest scales, topographic variation tends towards zero, and there is some contribution to σ_z at the largest scale due to the slightly concave or convex shape of the profile. Figure 5b presents this data as a cumulative percentage, which shows that the grain scale accounts for less than five percent of all topographic variation. This figure is the same as the Form Size Distribution (FSD) proposed by Nyander et al. (2003).

Using the TRC approach, we present the distribution of k_s predicted using Equation 1 in Figure 6a. Following the format of 'grain size distribution' and 'form size distribution', we term this style of plot the drag size distribution (DSD). There is
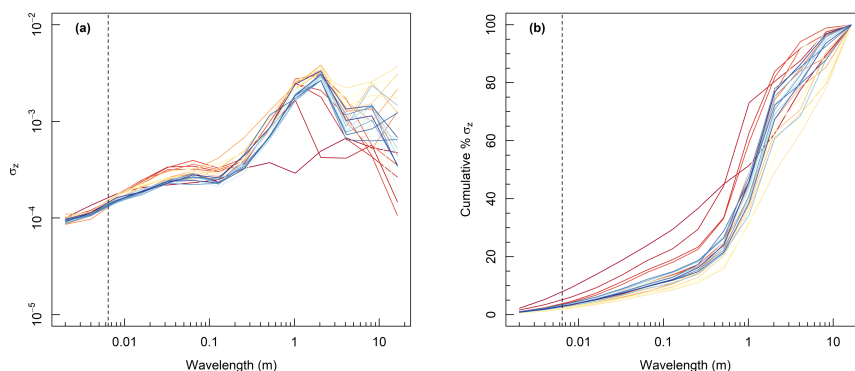
Figure 5. Form size distribution during Experiment 1a. Standard deviation of each topographic wavelength presented as an (a) absolute, and (b) cumulative percentage, for longitudinal profiles during the experiment. Refer to Figure 4 for legend.
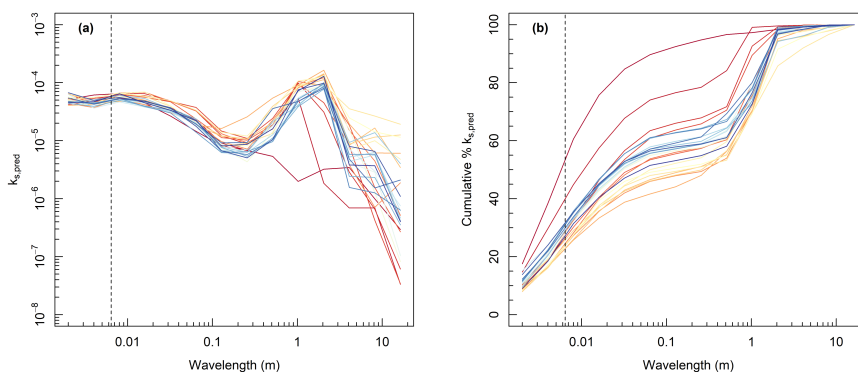

Figure 6. Drag size distribution during Experiment 1a. Estimated drag associated with each topographic wavelength presented as an (a) absolute, and (b) cumulative percentage, for longitudinal profiles during the experiment. Refer to Figure 4 for legend. Note that the absolute values of $k_{s,pred}$ appear unusually small for the surfaces ($\ll$ 1 mm) compared to values of σ_z, which is discussed later.

a major peak in the DSD at the scale of 2 m, and a minor peak at the scale of approximately 5 mm (around the size of the largest grains). At small scales, and large scales especially, estimated k_s tends downwards. Figure 6b presents the DSD as a cumulative percentage, which shows that the k_s associated with the grain scale is estimated to account for approximately 30 percent of the total k_s. This proportion of grain- and form-drag is similar to estimates in gravel-bed rivers with similar morphologies (Hey, 1988; Parker and Peterson, 1980; Prestegaard, 1983), which indicates that the TRC approach provides physically realistic estimates of drag.
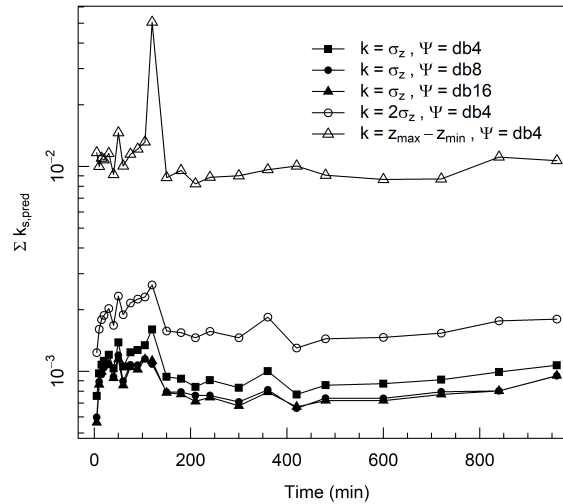
210

Earth **Surface**
Dynamics
Discussions

Figure 7. Sensitivity analysis of $\Sigma k_{s,pred}$ to choice of mother wavelet Ψ in MODWT and k in the roughness correlation for Experiment 1a, where $z_{max} - z_{min}$ is the maximum range of elevations. The combination of σ_z and Daubechies 4 wavelet is used in this study.

Figure 7 demonstrates the dependency of $\Sigma k_{s,pred}$ (i.e. sum of $k_{s,pred}$ for a given DEM) on the choice of mother wavelet and the k value in the roughness correlation. Various mother wavelets from the Daubechies family have been used when applying
215 wavelet transform to river bed topography (Nyander et al., 2003; Gutierrez et al., 2013; Qin et al., 2015), and for the same k value, these mother wavelets yield similar results. The values of $\Sigma k_{s,pred}$ are more sensitive to the choice of k. If standard deviation is used as the estimate of k, whilst changing Ψ, there is a relatively similar pattern of $\Sigma k_{s,pred}$. If the absolute range of elevations is used as k, as was used by (Forooghi et al., 2017), extreme outliers in the elevation profile disrupt a physically realistic pattern of total drag across the experiments, which should consist of at least an initial increase as the pool-bar-riffle
220 sequence emerges.

The approach of adding up the effect of different roughness elements to estimate a net effect, although established in the literature (Cowan, 1956; Einstein and Banks, 1950; Hey, 1988; Leopold et al., 1960; Millar, 1999), has been demonstrated to have limitations given that superimposed combinations of different roughness elements may produce drag feedbacks in either direction (Li, 2009; Wilcox and Wohl, 2006). Thus, it is important to demonstrate that $\Sigma k_{s,pred}$ is proportional to the total k_s.
225 Using data from all experiments conducted for this study, in addition to the step-pool experiments of Hohermuth and Weitbrecht (2018), Figure 8 compares the relationship between $\Sigma k_{s,pred}$ and the $k^*_{s,pred}$, the latter being the estimate of k_s obtained by applying the roughness correlation to the elevation profile without the transform. Each of the two datasets are described by a linear relationship, which demonstrates that both the transform and non-transform estimates of k_s are proportional. This validates the TRC approach for a given dataset, however, it is worth noting that the two datasets are characterised by different
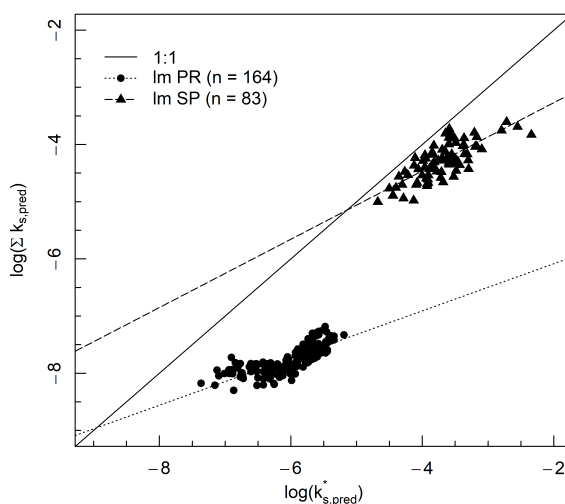
11

Figure 8. Relationship between $k^*_{s,pred}$ and $\Sigma k_{s,pred}$ for the pool-riffle (PR) experiments carried out for this study, as well as the step-pool (SP) experiments conducted by Hohermuth and Weitbrecht (2018).

slopes. The difference in slope likely arises due to the specific characteristics of each topographic dataset, which affect the wavelet decomposition of the wavelengths, and in turn, the values of $k_{s,pred}$. The choice of k in the roughness correlation does not affect the linear relationship between $k^*_{s,pred}$ and $\Sigma k_{s,pred}$.

Figure 9 compares the relationship between estimated flow resistance $(8/f)^{1/2}$ and relative submergence h/k, using two different values of k. In Figure 9a, relative submergence is calculated using σ_z, which is now common in gravel-bed rivers, whereas in Figure 9b, it is calculated using $k^*_{s,pred}$. Fergusons's (2007) variable-power equation (Appendix A) is applied with coefficients reported by Chen et al. (2020), which were fitted to a wide range of gravel-bed channels using $k = \sigma_z$. It is interesting to note that the $k^*_{s,pred}$ approach to relative submergence yields a closer fit to the Chen relation, quantified by a 30 percent smaller root-mean-square error. This result suggests that the estimates of k_s based on Equation 1 are useful in predicting flow resistance in rivers, and thus provides evidence for the multiscalar drag decomposition.

5 Implications for flow resistance in rivers

The roughness correlation developed by Forooghi et al. (2017) incorporates information regarding both the height of the roughness elements (a vertical roughness scale, Nikora et al. 1998) and the arrangement or spacing of roughness elements (a horizontal roughness scale, Bertin and Friedrich 2014). In isolation, either of these roughness scales may be misleading. For example, effective slope is a horizontal roughness metric and can be proportional to drag for some surfaces (Napoli et al.,
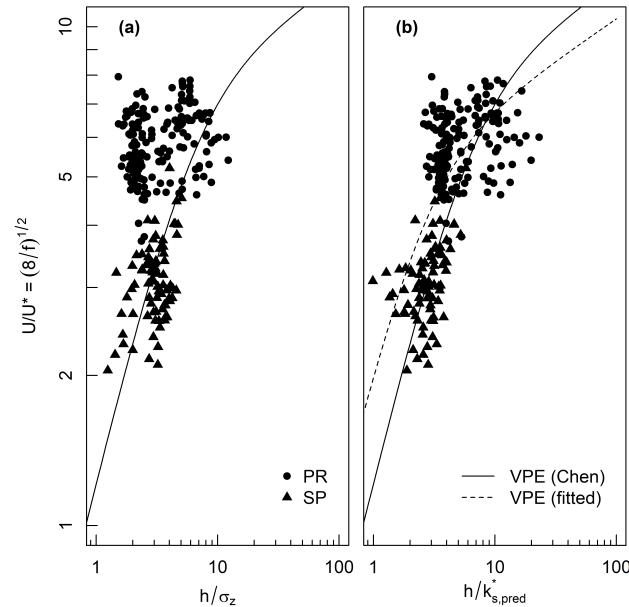
Figure 9. Plot of $(8/f)^{1/2}$ against relative submergence h/k, where (a) $k = \sigma_z$, and (b) $k = k_{s,pred}^*$. Solid line is the Ferguson (2007) variable-power equation (VPE) using coefficients $a_1 = 5.77$ and $a_2 = 1.24$ (Chen et al., 2020). Root-mean-square errors are 2.03 and 1.42, respectively. Dashed line is the VPE fitted to the data, where $a_1 = 4.81$ and $a_2 = 2.36$ (note: VPE could not be fitted to h/σ_z).

2008; Schultz and Flack, 2009). Thus, in isolation, Figure 4 would indicate that the small-scale bed features are most effective at producing drag. Alternatively, the standard deviation of surface elevations is a vertical roughness metric and has also shown to be proportional to flow resistance (Aberle et al., 1999; Chen et al., 2020). Therefore, in isolation, Figure 5 could lead to the interpretation that only the largest scale bed features produce drag. It is important to recognize that depending on the surface of interest, drag is usually a compromise between vertical and horizontal roughness, which is inherent in Equation 1 and the drag size distribution (Figure 6).

In gravel-bed rivers, which are typically ungauged, and where measurement of hydraulic variables is subject to practical limitations (Miller, 1958), flow resistance is typically estimated using only a vertical roughness scale. Upon introducing his method of sampling coarse bed material, Wolman (1954) remarked that these data could be used to estimate hydraulic roughness, and Lane (1957) agreed, based on the notion that grain diameter represents a vertical roughness scale as demonstrated by Nikuradse (1933). However, the relationship between grain diameter and flow resistance breaks down in natural channels for two main reasons: (1) grain diameter does not account for larger and often more hydrodynamically significant roughness elements (Sundborg, 1956; Leopold et al., 1964; Bathurst, 1982), and (2) it does not consider the horizontal spacing of these larger roughness elements (Schlichting, 1936; Nowell and Church, 1979; Davies and Sutherland, 1980), which has a systematic effect on drag (Morris, 1955; Leonardi et al., 2007; Napoli et al., 2008).

13

260   In recent years, the increased availability of high-resolution topographic data has led to the adoption of σ_z as a roughness scale, on the basis that it accounts for larger-scale bed structures (Aberle et al., 1999; Aberle and Smart, 2003; Cadol and Wohl, 2013; Smart et al., 2002; Yochum et al., 2014). However, σ_z only improves upon the first deficiency of grain-based roughness metrics, and consequently, it cannot be considered a measure of hydraulic roughness. The roughness correlation used herein may be a significant improvement over existing roughness metrics as it incorporates both vertical and horizontal roughness

265   scales, and provides a direct semi-empirical estimate of k_s. Moreover, roughness correlations of this variety can be applied to most datasets where σ_z is calculated.

6   Conclusions

The transform-roughness correlation approach allows researchers to estimate the relative contribution of various scales of bed topography to the total drag. By modifying the roughness correlation to suit the hydraulic conditions, multiscalar drag de-

270   composition may be achieved in virtually any type of river, and perhaps boundary-layers in other environments. The only requirement is that the topographic data is of a sufficient resolution and spatial extent to capture the scales over which the hydraulically-significant roughness elements occur, and data of this quality is only becoming more available to geomorphologists over time. In particular, we expect that given the continual advances in methods for collecting bathymetric data in both shallow (Kasvi et al., 2019) and deep channels (Dietrich, 2017), applying the TRC approach will become increasingly practical

275   in natural rivers.

    Given that the TRC approach may provide new and more detailed information regarding the effect of bed geometry on fluid dynamics, incorporating both horizontal and vertical scales of roughness, it may contribute to advances in hydraulics as well as an understanding of channel morphodynamics. The estimates of total k_s from semi-empirical roughness correlations may present more immediate benefits by serving as replacements for representative roughness values, which have historically been

280   necessitated by technological limitations.

    The application of the TRC approach herein demonstrates the limitations of commonly-used approaches to estimating flow resistance in rivers, which rely solely on representations of vertical roughness and ignore their horizontal arrangement. Also, it highlights the utility of wavelet transform as a tool that provides intuitive representations of channel bed topography. The TRC approach is currently being used to explore channel morphodynamics and bedload transport using laboratory experiments.

285   *Code and data availability.* Data and code are available online (https://doi.org/10.5281/zenodo.3879652; Adams (2020b)).

Earth **Surface**
Dynamics
Discussions

Appendix A: Ferguson (2007) variable-power equation

Ferguson (2007) presented the variable-power flow resistance equation

$$(8/f)^{1/2} = \frac{a_1 a_2 (h/k)}{(a_1^2 + a_2^2 (h/k)^{5/3})^{1/2}} \tag{A1}$$

where a_1 and a_2 are empirically-derived coefficients, h is flow depth or hydraulic radius, and k is some representative
290   roughness scale.

Author contributions. DLA is responsible for conceptualization, investigation, formal analysis, and writing. AZ provided expertise in open-channel flow, contributing to the interpretation and communication of the results and the proposed technique.

Earth **Surface**
Dynamics
Discussions

References

Aberle, J. E. and Smart, G. M.: The influence of roughness structure on flow resistance on steep slopes, Journal of Hydraulic Research, 41, 259–269, 2003.

300 Aberle, J. E., Dittrich, A., and Nestmann, F.: Description of steep stream roughness with the standard deviation s, in: Proceedings of the 28th Congress of the IAHR, Graz, Austria, 1999.

Adams, D. L.: Toward bed state morphodynamics in gravel-bed rivers, Progress in Physical Geography, https://doi.org/10.1177/0309133320900924, 2020a.

Adams, D. L.: Code and example data for transform-roughness correlation (TRC) approach, https://doi.org/doi.org/10.5281/zenodo.3879652, 305 2020b.

Addison, P. S.: Introduction to redundancy rules: the continuous wavelet transform comes of age, Philosophical Transactions of the Royal Society A: Mathematical, Physical and Engineering Sciences, 376, 1–15, https://doi.org/10.1098/rsta.2017.0258, 2018.

Ashworth, P. J. and Ferguson, R. I.: Size-selective entrainment of bed-load in gravel bed streams, Water Resources Research, 25, 627–634, https://doi.org/10.1029/WR025i004p00627, 1989.

310 Bathurst, J. C.: Flow resistance in boulder-bed streams, in: Gravel-bed rivers, edited by Hey, R. D., Bathurst, J. C., and Thorne, C. R., pp. 443–465, John Wiley & Sons, Chichester, U.K., 1982.

Bergeron, N. E.: Scale-space analysis of stream-bed roughness in coarse gravel-bed streams, Mathematical Geology, 28, 537–561, https://doi.org/10.1007/BF02066100, 1996.

Bertin, S. and Friedrich, H.: Measurement of Gravel-Bed Topography: Evaluation Study Applying Statistical Roughness Analysis, Jour-315 nal of Hydraulic Engineering, 140, 269–279, https://doi.org/10.1061/(ASCE)HY.1943-7900.0000823, http://ascelibrary.org/doi/10.1061/ {%}28ASCE{%}29HY.1943-7900.0000823, 2014.

Bray, D. I.: Flow resistance in gravel bed rivers, in: Gravel-bed rivers, edited by Hey, R. D., Bathurst, J. C., and Thorne, C. R., pp. 109–133, John Wiley & Sons, Chichester, U.K., 1982.

Buffington, J. M. and Montgomery, D. R.: A systematic analysis of eight decades of incipient motion studies, with special reference to 320 gravel-bedded rivers, Water Resources Research, 33, 1993–2029, https://doi.org/10.1029/97WR03138, 1997.

Cadol, D. and Wohl, E. E.: Variable contribution of wood to the hydraulic resistance of headwater tropical streams, Water Resources Research, 49, 4711–4723, https://doi.org/10.1002/wrcr.20362, 2013.

Cameron, S. M., Nikora, V. I., and Stewart, M. T.: Very-large-scale motions in rough-bed open-channel flow, Journal of Fluid Mechanics, 814, 416–429, https://doi.org/10.1017/jfm.2017.24, 2017.

325 Chen, X., Hassan, M. A., An, C., and Fu, X.: Rough correlations: Meta-analysis of roughness measures in gravel bed rivers, Water Resources Research, under review., 2020.

Chow, T. V.: Open channel hydraulics, McGraw-Hill Book Company, Inc, New York, 1959.

Church, M. A.: Rivers – Physical, Fluvial and Environmental Processes, Springer, https://doi.org/10.1007/978-3-319-17719-9, http://link. springer.com/10.1007/978-3-319-17719-9, 2015.

330 Clifford, N. J., Robert, A., and Richards, K. S.: Estimation of flow resistance in gravel-bedded rivers: A physical explanation of the multiplier of roughness length, Earth Surface Processes and Landforms, 17, 111–126, https://doi.org/10.1002/esp.3290170202, 1992.

Cowan, W. L.: Estimating hydraulic roughness coefficients., Agricultural Engineering, 7, 473–475, 1956.

Davies, T. R. H. and Sutherland, A. J.: Resistance to flow past deformable boundaries, Earth Surface Processes, 5, 175–179, 1980.

Dietrich, J. T.: Bathymetric Structure-from-Motion: extracting shallow stream bathymetry from multi-view stereo photogrammetry, Earth
335   Surface Processes and Landforms, 42, 355–364, https://doi.org/10.1002/esp.4060, http://doi.wiley.com/10.1002/esp.4060, 2017.

Eaton, B. C. and Church, M. A.: A graded stream response relation for bed load-dominated streams, Journal of Geophysical Research, 109,
    1–18, https://doi.org/10.1029/2003JF000062, 2004.

Eaton, B. C. and Church, M. A.: Channel stability in bed load-dominated streams with nonerodible banks: Inferences from experiments in a
    sinuous flume, Journal of Geophysical Research: Earth Surface, 114, 1–17, https://doi.org/10.1029/2007JF000902, 2009.

340 Einstein, H. A. and Banks, R. B.: Fluid resistance of composite roughness, Transactions of the American Geophysical Union, 31, 603–610,
    1950.

Ferguson, R. I.: Flow resistance equations for gravel- and boulder-bed streams, Water Resources Research, 43, 1–12,
    https://doi.org/10.1029/2006WR005422, 2007.

Field, J. P. and Pelletier, J. D.: Controls on the aerodynamic roughness length and the grain-size dependence of aeolian sediment transport,
345   Earth Surface Processes and Landforms, 43, 2616–2626, https://doi.org/10.1002/esp.4420, 2018.

Forooghi, P., Stroh, A., Magagnato, F., Jakirlic, S., and Frohnapfel, B.: Towards a Universal Roughness Correlation, Journal of Fluids
    Engineering, 139, 1–12, https://doi.org/10.1115/1.4037280, 2017.

Furbish, D. J.: Conditions for geometric similarity of coarse stream-bed roughness, Mathematical Geology, 19, 291–307,
    https://doi.org/10.1007/BF00897840, 1987.

350 Griffiths, G. A.: Flow resistance in coarse gravel bed rivers, Journal of the Hydraulics Division, 107, 899–918, 1981.

Gutierrez, R. R., Abad, J. D., Parsons, D. R., and Best, J. L.: Discrimination of bed form scales using robust spline filters and wavelet
    transforms: Methods and application to synthetic signals and bed forms of the Río Paraná, Argentina, Journal of Geophysical Research:
    Earth Surface, 118, 1400–1419, https://doi.org/10.1002/jgrf.20102, 2013.

Hey, R. D.: Flow Resistance in Gravel-Bed Rivers, Journal of the Hydraulics Division, 105, 365–379, 1979.

355 Hey, R. D.: Bar Form Resistance in Gravel-Bed Rivers, Journal of Hydraulic Engineering, 114, 1498–1508, 1988.

Hohermuth, B. and Weitbrecht, V.: Influence of Bed-Load Transport on Flow Resistance of Step-Pool Channels, Water Resources Research,
    54, 5567–5583, https://doi.org/10.1029/2017WR021523, 2018.

Jimenez, J.: Turbulent Flows over Rough Walls, Annual Review of Fluid Mechanics, 36, 173–196,
    https://doi.org/10.1146/annurev.fluid.36.050802.12210, 2004.

360 Kasvi, E., Salmela, J., Lotsari, E., Kumpula, T., and Lane, S. N.: Comparison of remote sensing based approaches for mapping bathymetry
    of shallow, clear water rivers, Geomorphology, 333, 180–197, https://doi.org/10.1016/j.geomorph.2019.02.017, https://doi.org/10.1016/j.
    geomorph.2019.02.017, 2019.

Keylock, C. J., Singh, A., and Foufoula-Georgiou, E.: The complexity of gravel bed river topography examined with gradual wavelet recon-
    struction, Journal of Geophysical Research: Earth Surface, 119, 682–700, https://doi.org/10.1002/2013JF002999, 2014.

365 Kumar, P. and Foufoula-Georgiou, E.: Wavelet Analysis for geophysical applications, Reviews of Geophysics, 34, 385–412,
    https://doi.org/10.1029/97RG00427, 1997.

Lane, E. W.: A study of the shape of channels formed by natural streams flowing in erodible material, Tech. rep., MRD Sediment Series no.
    9, United States Army Corps, Engineering Division, 1957.

Lee, A. J. and Ferguson, R. I.: Velocity and flow resistance in step-pool streams, Geomorphology, 46, 59–71, https://doi.org/10.1016/S0169-
370   555X(02)00054-5, 2002.

Leonardi, S., Orlandi, P., and Antonia, R. A.: Properties of d- and k-type roughness in a turbulent channel flow, Physics of Fluids, 19, 1–6, https://doi.org/10.1063/1.2821908, 2007.

Leopold, L. B., Bagnold, R. A., Wolman, M. G., and Bush, L. M.: Flow resistance in sinuous or irregular channels, Tech. rep., 1960.

Leopold, L. B., Wolman, M. G., and Miller, J. P.: Fluvial processes in geomorphology, Freeman, San Francisco, CA, 1964.

375   Li, G.: Preliminary study of the interference of surface objects and rainfall in overland flow resistance, Catena, 78, 154–158, https://doi.org/10.1016/j.catena.2009.03.010, 2009.

Limerinos, J. T.: Determination of the Manning Coefficient From Measured Bed Roughness in Natural Channels, Tech. rep., 1970.

MacKenzie, L. G. and Eaton, B. C.: Large grains matter: contrasting bed stability and morphodynamics during two nearly identical experiments, Earth Surface Processes and Landforms, 42, 1287–1295, https://doi.org/10.1002/esp.4122, 2017.

380   Millar, R. G.: Grain and form resistance in gravel-bed rivers, Journal of Hydraulic Research, 37, 303–312, https://doi.org/10.1080/00221686.1999.9628249, 1999.

Miller, J. P.: High mountain streams: Effects of geology on chanel characteristics and bed material, New Mexico State Bureau of Mines and Mine Resources Memoir 4, p. 51 pp., 1958.

Morris, H. M.: A new concept of flow in rough conduits, Transactions of the American Society of Civil Engineers, 120, 373–398, 1955.

385   Nanson, G. C. and Huang, H. Q.: Least action principle, equilibrium states, iterative adjustment and the stability of alluvial channels, Earth Surface Processes and Landforms, 33, 923–942, https://doi.org/10.1002/esp.1584, http://doi.wiley.com/10.1002/esp.1584, 2008.

Nanson, G. C. and Huang, H. Q.: A philosophy of rivers: Equilibrium states, channel evolution, teleomatic change and least action principle, Geomorphology, 302, 3–19, https://doi.org/10.1016/j.geomorph.2016.07.024, http://dx.doi.org/10.1016/j.geomorph.2016.07.024, 2018.

Napoli, E., Armenio, V., and De Marchis, M.: The effect of the slope of irregularly distributed roughness elements on turbulent wall-bounded

390   flows, Journal of Fluid Mechanics, 613, 385–394, https://doi.org/10.1017/S0022112008003571, 2008.

Nezu, I. and Nakagawa, H.: Turbulence in open-channel flows, IAHR Monograph Series, pp. 1–281, 1993.

Nield, J. M., King, J., Wiggs, G. F., Leyland, J., Bryant, R. G., Chiverrell, R. C., Darby, S. E., Eckardt, F. D., Thomas, D. S., Vircavs, L. H., and Washington, R.: Estimating aerodynamic roughness over complex surface terrain, Journal of Geophysical Research Atmospheres, 118, 12 948–12 961, https://doi.org/10.1002/2013JD020632, 2013.

395   Nikora, V. I., Goring, D. G., and Biggs, B. J. F.: On gravel-bed roughness characterization, Water Resources Research, 34, 517–527, https://doi.org/10.1029/97WR02886, 1998.

Nikuradse, J.: Laws of flow in rough pipes, Tech. rep., Washington, D. C., 1933.

Nowell, A. R. M. and Church, M. A.: Turbulent flow in a depth-limited boundary layer, Journal of Geophysical Research, 84, 4816–4824, https://doi.org/10.1029/JC084iC08p04816, 1979.

400   Nyander, A.: River-bed sediment surface characterisation using wavelet transform-based methods, Doctoral thesis, Napier University, 2004.

Nyander, A., Addison, P. S., McEwan, I., and Pender, G.: Analysis of river bed surface roughnesses using 2D wavelet transform-based methods, Arabian Journal for Science and Engineering, 28, 107–121, 2003.

Parker, G. and Peterson, A. W.: Bar Resistance of Gravel-Bed Streams, Journal of the Hydraulics Division, 106, 1159–1575, 1980.

Pelletier, J. D. and Field, J. P.: Predicting the roughness length of turbulent flows over landscapes with multi-scale microtopography, Earth

405   Surface Dynamics, 4, 391–405, https://doi.org/10.5194/esurf-4-391-2016, 2016.

Prestegaard, K. L.: Bar resistance in gravel bed streams at bankfull stage, Water Resources Research, 19, 472–476, https://doi.org/10.1029/WR019i002p00472, 1983.

Qin, J., Wu, T., and Zhong, D.: Spectral behavior of gravel dunes, Geomorphology, 231, 331–342, https://doi.org/10.1016/j.geomorph.2014.12.023, http://dx.doi.org/10.1016/j.geomorph.2014.12.023, 2015.

410 Robert, A.: Fractal properties of simulated bed profiles in coarse-grained channels, Mathematical Geology, 23, 367–382, https://doi.org/10.1007/BF02065788, 1991.

Robert, A. and Richards, K. S.: On the modelling of sand bedforms using the semivariogram, Earth Surface Processes and Landforms, 13, 459–473, https://doi.org/10.1002/esp.3290130510, 1988.

Schlichting, V. H.: Experimentelle untersuchungen zum Rauhigkeitsproblem, Archive of Applied Mechanics, 7, 1–34, 1936.

415 Schlichting, V. H.: Boundary-Layer Theory, McGraw-Hill, New York, 7th edn., 1979.

Schultz, M. P. and Flack, K. A.: Turbulent boundary layers on a systematically varied rough wall, Physics of Fluids, 21, 1–9, https://doi.org/10.1063/1.3059630, 2009.

Smart, G. M., Duncan, M. J., and Walsh, J. M.: Relatively Rough Flow Resistance Equations, Journal of Hydraulic Engineering, 128, 568–578, https://doi.org/10.1061/(ASCE)0733-9429(2002)128:6(568), 2002.

420 Sundborg, A.: The River Klarälven: A Study of Fluvial Processes, Geografiska Annaler, 38, 125–237, 1956.

Torrence, C. and Compo, G. P.: A practical guide to wavelet analysis, Bulletin of the American Meteorological society, 79, 61–78, 1998.

Weichert, R. B., Bezzola, G. R., and Minor, H.-E.: Bed erosion in steep open channels, Journal of Hydraulic Research, 47, 360–371, https://doi.org/10.3826/jhr.2009.3128, 2009.

Westoby, M. J., Brasington, J., Glasser, N. F., Hambrey, M. J., and Reynolds, J. M.: 'Structure-from-Motion' photogrammetry: A low-cost,
425 effective tool for geoscience applications, Geomorphology, 179, 300–314, https://doi.org/10.1016/j.geomorph.2012.08.021, 2012.

Wilcox, A. C. and Wohl, E. E.: Flow resistance dynamics in step-pool stream channels: 1. Large woody debris and controls on total resistance, Water Resources Research, 42, 1–16, https://doi.org/10.1029/2005WR004277, 2006.

Wolman, M. G.: A method of sampling coarse river-bed material, Transactions, American Geophysical Union, 35, 951–956, 1954.

Wolman, M. G. and Miller, J. P.: Magnitude and Frequency of Forces in Geomorphic Processes, The Journal of Geology, 68, 54–74, 1960.

430 Yochum, S. E., Bledsoe, B. P., Wohl, E. E., and David, G. C. L.: Spatial characterization of roughness elements in high-gradient channels of the Fraser Experimental Forest, Colorado, USA, Water Resources Research, 50, 6015–6029, https://doi.org/10.1002/2014WR015587, 2014.